

# Unraveling the Effects of Size, Composition, and Substrate on the Localized Surface Plasmon Resonance Frequencies of Gold and Silver Nanocubes: A Systematic Single-Particle Approach

Emilie Ringe,<sup>†</sup> Jeffrey M. McMahon,<sup>†</sup> Kwonnam Sohn,<sup>‡</sup> Claire Cobley,<sup>§</sup> Younan Xia,<sup>§</sup> Jiaxing Huang,<sup>‡</sup> George C. Schatz,<sup>†</sup> Laurence D. Marks,<sup>‡</sup> and Richard P. Van Duyne<sup>\*,†</sup>

Department of Chemistry, Northwestern University, Evanston, Illinois 60208, Department of Materials Science and Engineering, Northwestern University, Evanston, Illinois 60208, and Department of Biomedical Engineering, Washington University, St. Louis, Missouri 63130

Received: May 13, 2010; Revised Manuscript Received: June 25, 2010

Localized surface plasmon resonances (LSPRs), resulting from the interaction of light with metal nanoparticles, are powerful tools for biological sensors, surface-enhanced spectroscopies, and optical devices. LSPR frequencies are strongly dependent on a nanoparticle's structure, composition, and local dielectric environment. However, these relationships are prohibitively difficult or impossible to probe from bulk solutions due to the heterogeneity of chemically synthesized products. In this study, systematic single-particle structure–property measurements, coupled with a statistical analysis and FDTD calculations, are performed on silver and gold nanocubes. The dependencies of LSPR frequencies on nanocube size, composition, and substrate dielectric constant are determined. The results obtained represent the most quantitative measurements and analysis to date, yielding predictive rules and fundamental insights into the interactions between nanoparticles and substrates.

## 1. Introduction

The optical properties of nanoparticles have been observed for centuries, for example, as part of strikingly colored stained glass. In recent decades, applications of these have exploded, from biological and chemical sensors,<sup>1–4</sup> to waveguides,<sup>5,6</sup> to tools for surface-enhanced spectroscopies<sup>7–9</sup> and second harmonic generation.<sup>10–12</sup> The phenomena behind such optical properties are localized surface plasmon resonances (LSPRs), collective electron oscillations on their surface, which are capable of strongly scattering light. The versatile nature of LSPRs can be attributed to their strong dependence on a nanoparticle's composition, shape, size, and local dielectric environment.<sup>13–22</sup>

One of the features of LSPRs particularly important to a myriad of sensing devices,<sup>3,23,24</sup> and to this work, is the sensitivity of their frequencies to the local dielectric environment, such as the substrate.<sup>13–15,19,20</sup> This relationship has rarely received systematic investigation,<sup>13,21,22,25,26</sup> except in our previous work<sup>13,25</sup> where some initial aspects of this were studied using single Ag nanocubes. There, it was demonstrated that the interaction of a nanoparticle (specifically, a nanocube) with a substrate can cause its LSPRs to be dramatically affected, such as excitations of both dipolar and higher-order ones.<sup>13</sup> Additionally, these interactions were found to be sensitive to details at the 1 nm level.<sup>25</sup> To the best of our knowledge, such behavior has never been analyzed using measurements on a collection of single nanoparticles, which is important in order to make more generalized statements about the interaction of a nano-

particle with a substrate. Another feature that has not received much attention, at least at the single-particle level, is the effect of nanoparticle composition on this interaction, such as the relative sensitivities of silver (Ag) LSPRs compared to gold (Au).

In this article, we expand on our previous work<sup>13,25</sup> and elucidate general relationships between the optical properties of an isolated nanoparticle and its size, composition, and local dielectric environment. Both Ag and Au nanocubes are studied on Formvar (a polymer) and Si<sub>3</sub>N<sub>4</sub> (a semiconductor) substrates, using a robust structure–function correlation technique.<sup>25,27</sup> Optical responses are measured using dark-field scattering spectroscopy, corresponding structural information is obtained using high-resolution transmission electron microscopy (HR-TEM), and a theoretical analysis is provided through finite-difference time-domain (FDTD) calculations.

## 2. Methods

**2.1. Experimental.** Cetyltrimethylammonium bromide (CTAB)-capped single-crystalline Au nanocubes were prepared following a previously reported procedure<sup>28</sup> involving the reduction of HAuCl<sub>4</sub> trihydrate by ascorbic acid. Poly(vinylpyrrolidone) (PVP)-capped single-crystalline Ag nanocubes were synthesized using a previously reported modified polyol method,<sup>29</sup> where trace amounts of sodium hydrosulfide are added to a typical polyol reduction of AgNO<sub>3</sub>, which results in a high yield of uniform nanocubes.

Two types of TEM support films were used: Formvar (polyvinyl formal) and silicon nitride. Formvar refers to ultrathin carbon type A grids, copper grids coated with a 30–60 nm thick layer of Formvar on one side, and a layer of amorphous carbon (3–4 nm) on the other side. The particles have been applied on the Formvar side, and such films can be considered to have a constant refractive index (RI) of  $n = 1.5$ .<sup>30</sup> Silicon nitride

\* To whom correspondence should be addressed. E-mail: vanduyne@northwestern.edu.

<sup>†</sup> Department of Chemistry, Northwestern University.

<sup>‡</sup> Department of Materials Science and Engineering, Northwestern University.

<sup>§</sup> Washington University.

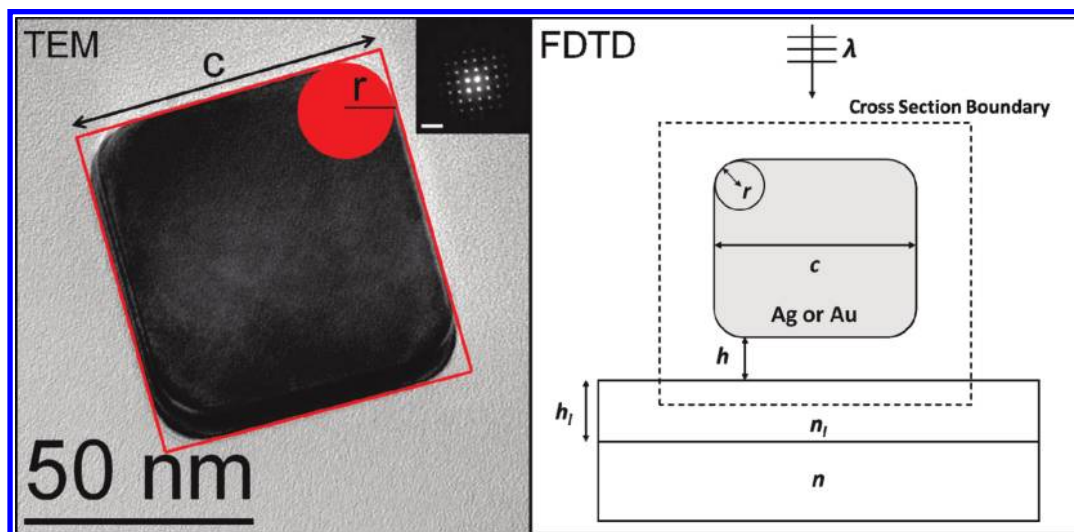


**Figure 1.** (left) HRTEM image of a Ag nanocube and definition of its structural parameters:  $c$ , the face-to-face distance, and  $r$ , the radius of curvature. The nanodiffraction pattern (inset) shows alignment along the [100] zone axis. The scalebar of the nanodiffraction pattern is  $10 \text{ nm}^{-1}$ . (right) Schematic diagram of the system considered in the FDTD calculations. The parameters in the figure are defined in the text.

films with an approximate stoichiometry of  $\text{Si}_3\text{N}_4$  and a 100 nm thickness were also used. It can be assumed that these films have a constant RI of  $n = 2.05$ , but this value can range from 1.9 to 2.1 depending on the actual stoichiometry (nonstoichiometric films are more easily manufactured and yield lower-stress membranes preferred for TEM use).<sup>31,32</sup>

A 1–5  $\mu\text{L}$  drop of an aqueous suspension of the nanocubes was put on a support film and dried in air. TEM grids were then deposited on a clean glass coverslip (RI of  $n = 1.5$ ) and dark-field scattering was used to obtain LSPR spectra, following a previously reported procedure.<sup>27</sup> LSPR positions were obtained by fitting the spectra to Lorentzian curves.

HRTEM images were obtained within days of the optical characterization on either a JEOL JEM2100 FAST TEM or a Hitachi HD-2300A scanning TEM, both operated at 200 kV. The sizes and corner rounding of the nanocubes were obtained from these images. The obtainable subnanometer resolution gives small error margins of only 0.5 and 1 nm (approximately) for the sizes and corner rounding, respectively. In this context, size is defined as the face-to-face distance ( $c$ ), and corner rounding is defined as the radius of a circle that can be inscribed on the corner of the nanocube's image ( $r$ ); see Figure 1. Only nanocubes with a projected aspect ratio between 0.90 and 1.11, isotropic rounding, and average relative rounding ( $r/c$ ) of the corners visible in the HRTEM image of less than 0.22 were considered. A total of 42, 58, 52, and 23 nanocubes fulfilled these conditions for Ag on Formvar, Ag on  $\text{Si}_3\text{N}_4$ , Au on Formvar, and Au on  $\text{Si}_3\text{N}_4$ , respectively.

**2.2. Computational.** FDTD calculations were performed using standard techniques.<sup>33</sup> Systems were modeled directly after the experiments: nanocubes specified by  $c$  and  $r$  were placed a distance  $h$  above an infinitely thick or layered substrate. A schematic diagram of the modeled system is presented in Figure 1. Infinitely thick films of Formvar or  $\text{Si}_3\text{N}_4$  were considered to have constant RIs of  $n = 1.5$  or 2.05, respectively. For calculations involving a layered substrate, a  $\text{Si}_3\text{N}_4$  layer with thickness  $h_1 = 25\text{--}200 \text{ nm}$  and RI of  $n_1 = 2.05$  was placed atop an infinite glass (RI of  $n = 1.5$ ) layer. The nanocubes were illuminated from above at normal incidence using a Gaussian damped sinusoidal pulse with a wavelength content over the range of interest (300–1000 nm). Optical responses were determined from normalized scattering cross sections, calculated

by integrating the normal component of the Poynting vector over an enclosing surface.<sup>34</sup>

Computational domains were variable in size, depending on the particular nanocube under consideration. Unless otherwise specified, domains were discretized using grid spacings of 0.5 nm in all directions and truncated using convolutional perfectly matched layers. On the basis of previous calculations,<sup>25</sup> such spacings are sufficient to accurately model the considered systems and are capable of resolving differences at the  $\pm 1 \text{ nm}$  level (approximately the same resolution as the HRTEM images). We mention in passing that convergence with respect to grid spacing is an important point that can often be challenging when using numerical methods.<sup>35</sup>

The dielectric functions of Ag and Au were modeled using Drude plus two Lorentz pole oscillator models<sup>25</sup> fit to experimentally determined data<sup>36</sup> over the wavelength range important to this study.

### 3. Results and Discussion

We first studied the effects of changes in nanocube composition and substrate dielectric constant on LSPR spectra by performing correlated LSPR/HRTEM measurements<sup>27</sup> on four different sets of nanocubes: Ag on Formvar, Ag on  $\text{Si}_3\text{N}_4$ , Au on Formvar, and Au on  $\text{Si}_3\text{N}_4$ . When all other factors are kept the same, direct comparisons between Au and Ag, as well as Formvar and  $\text{Si}_3\text{N}_4$ , can be made. Representative dark-field scattering spectra of Au and Ag nanocubes on Formvar and  $\text{Si}_3\text{N}_4$  are presented in Figure 2. To directly probe the relationship between nanoparticle composition and substrate dielectric properties, nanocubes of similar sizes and comparable corner roundings were chosen:  $c = 78.4, 76.1, 78.3,$  and  $77.3 \text{ nm}$  and  $r = 12, 12, 14,$  and  $10 \text{ nm}$  for a Ag nanocube on Formvar, Ag nanocube on  $\text{Si}_3\text{N}_4$ , Au nanocube on Formvar, and Au nanocube on  $\text{Si}_3\text{N}_4$ , respectively.

In the Ag spectra, two peaks are observed: a sharp one near 400 nm and a broad one near 500 nm.<sup>13,25</sup> The former can be attributed to a quadrupolar LSPR localized to the corners of the nanocube, whereas the latter can be considered a dipolar one localized along the sides.<sup>25</sup> FDTD calculated profiles of the electric field intensities at the wavelengths of the two resonances for the nanocube on Formvar reveals some additional informa-

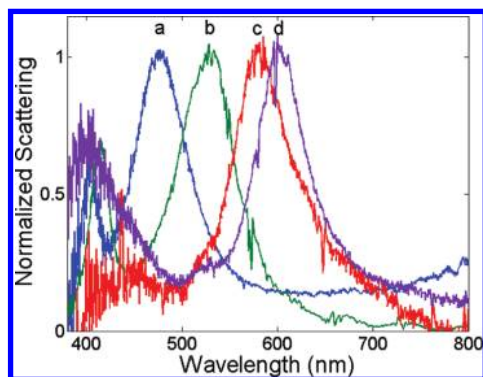


**Figure 2.** Effect of composition and substrate on the dark-field scattering of nanocubes of similar sizes and corner roundings: (a) Ag on Formvar,  $\lambda_{\max} = 475$  nm; (b) Ag on  $\text{Si}_3\text{N}_4$ ,  $\lambda_{\max} = 524$  nm; (c) Au on Formvar,  $\lambda_{\max} = 583$  nm; and (d) Au on  $\text{Si}_3\text{N}_4$ ,  $\lambda_{\max} = 603$  nm.

tion; see Figure 3 for both the FDTD calculated spectrum and the field profiles. In particular, the quadrupolar LSPR has correlations with fields that extend into the lower RI material, whereas the dipolar one has correlations with the higher RI environment (which, in this case, are air and substrate, respectively). In the presence of a substrate that has a higher RI than the surrounding material, these resonances can, therefore, be classified as “proximal” (near the substrate) or “distal” (away from it).<sup>13</sup> Because all systems considered herein satisfy this condition, these resonances will hereon be referred to as such. It is important to note that the wavelengths that these modes occur at and their correlations are dependent on the actual RIs of the substrate and surrounding medium, and not simply the difference between the two.

One of the big differences between the Ag and Au nanocubes is that the distal LSPR is not observed for the latter (Figure 2). This is because its wavelength falls in the interband transition region (below approximately 500 nm). Thus, only the proximal LSPR in the case of Au (near 600 nm) is relevant to the current study. The distal LSPR in Au nonetheless exists and is expected to red shift upon increase of the substrate RI. Indeed, a band near 525 nm is noticeable in the spectra for the Au nanocube on  $\text{Si}_3\text{N}_4$ , which is potentially the distal LSPR. Work on higher RI substrates is currently underway to confirm this assignment. Because the distal plasmon mode is not prominently present in Au, it is expected that, if nanocubes were to be immobilized on a substrate, only Ag ones would be useful for applications (e.g., sensing) that involve the upper surrounding medium.

However, both the Ag and the Au nanocubes exhibit strong proximal LSPRs and thus are both expected to be sensitive to the substrate’s dielectric properties. To better understand the effect of changing these properties, optical responses of Au nanocubes sitting directly ( $h = 0$ ) on Formvar or  $\text{Si}_3\text{N}_4$  were determined both experimentally and using FDTD; see Figure 4. Two nanocubes were chosen, and detailed structural parameters were obtained from HRTEM images (not shown); the one on Formvar had  $c = 84.0$  nm and  $r = 15.2$  nm, whereas the one on  $\text{Si}_3\text{N}_4$  had  $c = 74.2$  nm and  $r = 12.7$  nm. Figure 4 demonstrates that the major effects of increasing the substrate’s RI are that the proximal LSPR is red shifted (by approximately 40 nm for these particular nanocubes) and becomes slightly narrower. Such behavior is not unreasonable given the correlation of the proximal LSPR mode with the substrate (as discussed above) and can be generalized to other nanoparticles. It is expected that other LSPR modes, including distal resonances (such as those in Ag), would be less affected by a change of substrate. We will return to these points below.

Comparison of the experimental and calculated spectra yields excellent agreement for the  $\text{Si}_3\text{N}_4$  results; see Figure 4. Such agreement indicates that our choice of  $n = 2.05$  for the RI of nonstoichiometric  $\text{Si}_3\text{N}_4$  was correct. However, there are some discrepancies. The one in the interband transition region can be attributed to the low intensity of the white light at short wavelengths in the experiments, rendering the results in that region less reliable. Another one is that the calculation shows a sharp dip to zero intensity near 720 nm that is not seen experimentally. This feature is caused by an optical mode in the  $\text{Si}_3\text{N}_4$  layer (see below), which presumably does not arise in the experiments due to sample imperfections and inhomogeneities in thickness.

The Formvar results in Figure 4 also yield good agreement, except for a slight shape mismatch of the proximal LSPR and the fact that the calculation suggests it should occur 10 nm to the blue. This is understandable, considering that the FDTD calculations assume that there are no contaminants on the surface of the nanocubes, which could create a higher local dielectric environment that would lead to a relative blue shift of the results. This would not have as significant of an effect on the  $\text{Si}_3\text{N}_4$  results, where the substrate RI is already high. This explanation is more likely than other possible ones, such as chemical interactions between a nanocube and the substrate, which are expected to have little effect.

To investigate the impact that the thickness of the substrate has, optical responses of Au nanocubes with  $c = 72$  nm and  $r = 11$  nm placed directly on  $\text{Si}_3\text{N}_4$  layers of varying heights ( $h_1 = 25$ –200 nm), all atop infinite glass substrates, were calculated; see Figure 5. Note that, for these calculations, grid spacings of 1.0 nm were used, as fine details are less important here than in the other results presented. As soon as the  $\text{Si}_3\text{N}_4$  layer is added ( $h_1 = 25$  nm), the proximal LSPR shifts from 557 to 607 nm, equivalent to that found when changing the RI of an infinite layer from  $n = 1.5$  to  $n = 2$  (see below). Further increasing  $h_1$  does not affect the position of the proximal LSPR, showing that only the RI of the material in the very near-field of the nanoparticle is important regarding its excitation. As the thickness of  $\text{Si}_3\text{N}_4$  is increased, an optical mode in this layer grows in intensity and is fully sustained around 75–100 nm, which is seen as a minimum going to zero in intensity at approximately 800 nm (meaning that all scattering from the nanocube enters this mode), followed by a broad maximum. Confirmation of the nature of this mode comes from its behavior with changing  $h_1$ . As the  $h_1$  is further increased, the optical mode red shifts, eventually leaving the spectral range considered. One interesting side effect of this mode is that, when it is initially sustained, the proximal LSPR appears sharp relative to the infinite substrate due to the drop to zero in intensity. This effect also causes the same LSPR to be broader when the optical mode red shifts to long wavelengths (see the  $h_1 = 200$  nm results, for example). Also interesting is that, for thicknesses of both 100 and 200 nm, a peak near 400 nm is observed, which is likely unrelated to interband transitions, but could be attributed to an LSPR, or possibly another optical mode altogether.

Another factor that can have a significant effect on the optical response of a nanoparticle is its distance from the substrate. In the present experiments, intuition tells us that the presence of molecules, such as surfactants or contaminants, on a nanocube surface will create some separation. Because this is hard to probe experimentally, we used FDTD to calculate optical responses for a Au nanocube with  $c = 84.0$  nm and  $r = 15.0$  nm at different distances  $h$  from a Formvar substrate. The proximal LSPR shifts significantly as the nanocube is brought closer to

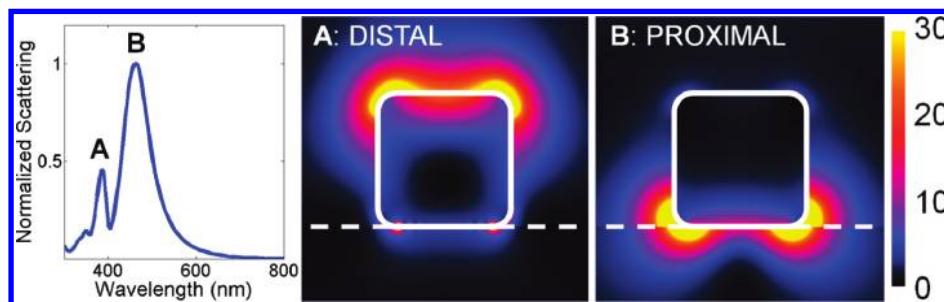


**Figure 3.** FDTD calculated optical response (left) and electric field intensities for the (A, 388 nm) distal and (B, 467 nm) proximal LSPRs for a  $c = 78$  nm and  $r = 12$  nm Ag nanocube. In the field profiles, the nanocube is outlined in solid white, and the substrate position is indicated using a dashed white line.

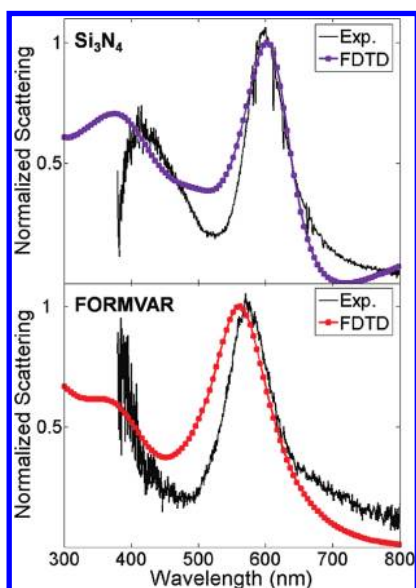


**Figure 4.** Comparison of (line and symbols) FDTD calculated and (line only) experimental scattering for Au nanocubes on (top) Formvar and (bottom)  $\text{Si}_3\text{N}_4$ . Structural parameters for the nanocubes are discussed in the text.

the substrate, from 542 nm when infinitely separated (isolated in air), to 552 nm when  $h = 2$  nm, to 562 nm when directly in contact with it ( $h = 0$ ); see Figure 6. Note that the term “proximal LSPR” is used loosely in this context, as such a definition does not make sense without the presence of a near-field substrate (see above). Therefore, this term should be considered synonymous with the term “dipolar LSPR”. The results obtained are in agreement with both previous studies on Ag nanocubes without corner rounding<sup>13</sup> and the discussion above, further suggesting that only the near-field proximity of a material, often just a few nanometers, is influential on the proximal LSPR.

Most of the effects thus far discussed can be qualitatively understood by comparing a few nanocubes, as we have done up to this point. However, to quantitatively elucidate them, we performed a large number of LSPR/HRTEM measurements and statistically analyzed the results. Note that only nanocubes with a relative rounding ( $r/c$ ) of less than 0.22 were included in the following because an average blue shift of 0.08 eV was observed between these and those with a higher relative rounding (not shown).

One of the things that we wish to revisit with the statistical analysis is the sensitivity of the proximal LSPR to substrate RI and its relation to nanocube composition. Figure 7 shows the proximal LSPR positions (energies) for Ag and Au nanocubes on Formvar and  $\text{Si}_3\text{N}_4$  for various side lengths. Figure 8 shows

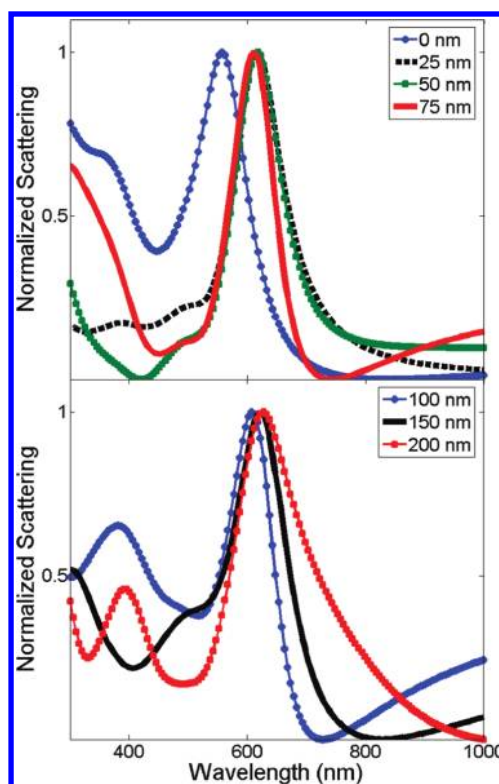


**Figure 5.** Effect of substrate thickness on the optical response of a Au nanocube calculated using FDTD. The nanocube is directly atop a  $\text{Si}_3\text{N}_4$  substrate on an infinite glass medium. (top) Red shift of the proximal LSPR due to the introduction of a high RI substrate, and the buildup of an optical mode with increasing thickness. (bottom) Red shift of the optical mode with a further increase of thickness.

an analogous plot for only Ag, displaying results for both the proximal and the distal LSPRs. The most prominent result in Figure 7 is that the proximal LSPRs are significantly red shifted for Au relative to Ag. Consider a  $c = 85$  nm nanocube, for example. The Ag and Au LSPRs are separated by 0.43 and 0.26 eV on Formvar and  $\text{Si}_3\text{N}_4$ , respectively. This trend is qualitatively expected and consistent with both Mie theory<sup>37</sup> and previously published experimental results for spherical nanoparticles.<sup>16</sup> More interesting is that the red shift in LSPR position with increase in substrate RI is both constant and predictable for all LSPRs under consideration (Au proximal, Ag proximal, and Ag distal). This result was qualitatively studied above. However, the quantitative information provided here reveals a more complex situation in which the magnitude of the red shift depends on both the nanocube composition and the type of LSPR. Specifically, going from an RI of 1.5 to 2.05 shifts the Au proximal, Ag proximal, and Ag distal LSPRs by an average of 0.057, 0.23, and 0.053 eV, respectively. The difference in

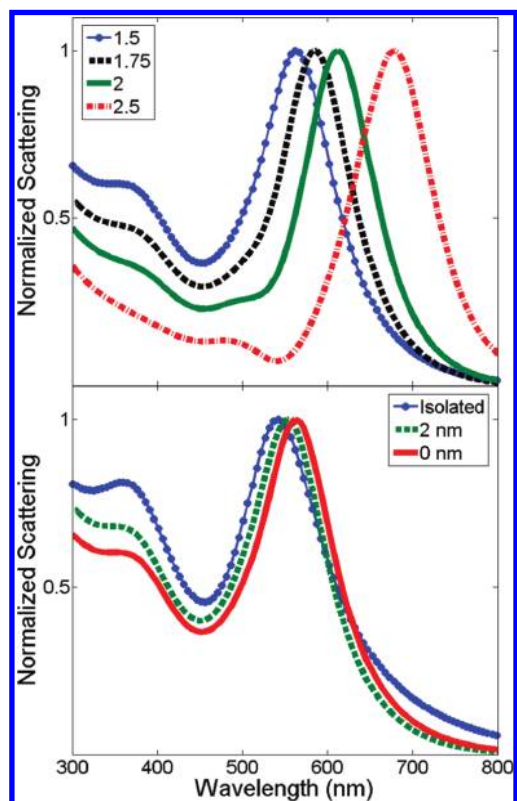


**Figure 6.** Effect of the substrate on the optical response of a Au nanocube, calculated using FDTD. (top) Optical responses for various substrate RI values. The nanocube is resting directly atop the substrate. (bottom) Optical responses of a nanocube as it is displaced a certain distance from a Formvar substrate.

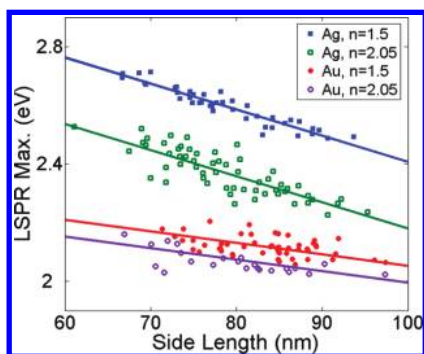


**Figure 7.** Effect of nanocube composition and substrate RI on the proximal LSPR positions of Ag and Au nanocubes. Parallel-fit lines are shown, as explained in the text. The differences in LSPR positions on Formvar and  $\text{Si}_3\text{N}_4$  are 0.23 and 0.057 eV for Ag and Au, respectively.

sensitivity between the proximal LSPRs of Ag and Au can be related to the change in the real part of their dielectric constants with the substrate dielectric value (which is larger in magnitude for Ag).<sup>38</sup> The difference in RI sensitivity between the proximal and distal LSPRs of Ag, on the other hand, can be explained by their different local environment correlations (the substrate and surrounding dielectric medium, respectively), as discussed above. An interesting feature of these results is that the red shifts are independent of nanocube size for a given LSPR, suggesting that a heterogeneous collection of nanocubes would not affect their performance if used in an application based on the sensitivity to substrate RI, for example.

From the correlated LSPR/HRTEM data in Figures 7 and 8, we can directly study the effect of size on the LSPR positions. A significant linear relationship between the LSPR position and

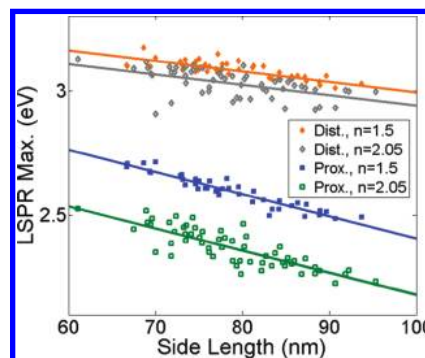


**Figure 8.** Effect of substrate RI on the distal and proximal LSPRs of Ag nanocubes. Parallel-fit lines are shown for each LSPR, as explained in the text. The differences in positions on Formvar and  $\text{Si}_3\text{N}_4$  are 0.053 and 0.23 eV for the distal and proximal LSPRs, respectively. Note that the data for the proximal LSPRs are identical to that in Figure 7.

**TABLE 1: Fit Parameters and  $p$ -Values for the Size Dependence of the LSPR Positions of Ag and Au Nanocubes. The Data Are Presented in Figures 7 and 8<sup>a</sup>**

sample (LSPR)	substrate	slope meV/nm	intercept eV	$p$ -value
Au (proximal)	$\text{Si}_3\text{N}_4$	-3.9 (0.6)	2.39 (0.05)	0.37
Au (proximal)	Formvar		2.44 (0.05)	
Ag (distal)	$\text{Si}_3\text{N}_4$	-4.2 (0.6)	3.36 (0.05)	0.63
Ag (distal)	Formvar		3.41 (0.05)	
Ag (proximal)	$\text{Si}_3\text{N}_4$	-8.9 (0.5)	3.07 (0.04)	0.65
Ag (proximal)	Formvar		3.30 (0.04)	

<sup>a</sup> Standard deviations are shown in parentheses.

the nanocube side length was found for all three resonances under consideration. Statistics were obtained using analysis of covariance, a tool for analyzing groups of data which may have different slopes, relating response (LSPR position) and predictor (side length) variables. The slope of the LSPR positions as a function of size was found to not be statistically different for a given peak on either substrate, having  $p$ -values of 0.37, 0.63, and 0.65 for Au proximal, Ag distal, and Ag proximal, respectively; see Table 1. Note that a  $p$ -value is related to the probability that the difference between two groups is the result of chance, which goes from 0 (not likely, or in other words a real effect) to 1 (extremely likely). Thus, a model constraining the slopes to be the same (parallel lines) was used for subsequent analysis and is shown as such in Figures 7 and 8. The results obtained, together with their standard deviations, are presented in Table 1. The small standard deviations on these results suggest that they are at a level where they can challenge and help improve theory. It can be seen that the dependence of the LSPR position on nanocube size is greatest for the Ag proximal LSPR, followed by Ag distal, and then by Au proximal. Perhaps the most novel result to come out of this analysis is that the quantitative nature of it can be used to predict LSPR positions of nanocubes over a large range of sizes, and of different compositions (Au or Ag), as well as on different substrates (Formvar or  $\text{Si}_3\text{N}_4$ ).

#### 4. Conclusions

A systematic study of Ag and Au nanocubes was performed. Both qualitative and predictive rules for LSPR behavior as a function of nanocube size, composition, and substrate were obtained experimentally and computationally. The results presented suggest that such LSPRs could be especially useful for applications based on RI sensing. In particular, the distal LSPR of Ag nanocubes is a prime candidate, as it is rather sharp

and has a relatively weak dependence on position with nanocube size (Figure 7), meaning slight heterogeneities would be insignificant. Additionally, on the basis of its correlations, the distal LSPR is expected to have a high sensitivity to changes in RI above the substrate, while having a low sensitivity to the substrate itself.<sup>13</sup>

**Acknowledgment.** Experimental characterization work was performed by E.R. FDTD calculations were performed by J.M.M. HRTEM work was performed in the EPIC facility of the NUANCE Center at Northwestern University, supported by NSF-NSEC, NSF-MRSEC, the Keck Foundation, the State of Illinois, and Northwestern University. This work was supported by the NSF (EEC-0647560, CHE-0414554, CHE-0911145, BES-0507036, and DMR-0804088), AFOSR/DARPA Project BAA07-61 (FA9550-08-1-0221), AFOSR DURIP (FA9550-07-1-0526), DTRA JSTO (FA9550-06-1-0558), and the NSF MRSEC (DMR-0520513) at the Materials Research Center of Northwestern University.

## References and Notes

- (1) Shon, Y.-S.; Choi, H. Y.; Guerrero, M. S.; Kwon, C. *Plasmonics* **2009**, *4*, 95.
- (2) Anker, J. N.; Hall, W. P.; Lyandres, O.; Shah, N. C.; Zhao, J.; Van Duyne, R. P. *Nat. Mater.* **2008**, *7*, 442.
- (3) Willets, K. A.; Van Duyne, R. P. *Annu. Rev. Phys. Chem.* **2007**, *58*, 267.
- (4) Haes, A. J.; Stuart, D. A.; Nie, S.; Van Duyne, R. P. *J. Fluoresc.* **2004**, *14*, 355.
- (5) Atwater, H. A. *Sci. Am.* **2007**, *296*, 56.
- (6) Dionne, J. A.; Sweatlock, L. A.; Atwater, H. A.; Polman, A. *Phys. Rev. B* **2006**, *73*, 035407.
- (7) Kahl, M.; Voges, E.; Kostrewa, S.; Viets, C.; Hill, W. *Sens. Actuators, B* **1998**, *51*, 285.
- (8) Lakowicz, J. R.; Geddes, C. D.; Gryczynski, I.; Malicka, J.; Gryczynski, Z.; Alsan, K.; Lukomska, J.; Matveeva, E.; Zhang, J.; Badugu, R.; Huang, J. *J. Fluoresc.* **2004**, *14*, 425.
- (9) Stiles, P. L.; Dieringer, J. A.; Shah, N. C.; Van Duyne, R. P. *Annu. Rev. Anal. Chem.* **2008**, *1*, 601.
- (10) Hao, E. C.; Schatz, G. C.; Johnson, R. C.; Hupp, J. T. *J. Chem. Phys.* **2002**, *117*, 5963.
- (11) Podlipensky, A.; Lange, J.; Seifert, G.; Graener, H.; Cravetchi, I. *Opt. Lett.* **2003**, *28*, 716.
- (12) Chen, C. K.; Heinz, T. F.; Ricard, D.; Shen, Y. R. *Phys. Rev. B* **1983**, *27*, 1965.
- (13) Sherry, L. J.; Chang, S.-H.; Schatz, G. C.; Van Duyne, R. P.; Wiley, B. J.; Xia, Y. *Nano Lett.* **2005**, *5*, 2034.
- (14) Itoh, T.; Uwada, T.; Asahi, T.; Ozaki, Y.; Masuhara, H. *Can. J. Anal. Sci. Spectrosc.* **2007**, *52*, 130.
- (15) Murray, W. A.; Auguie, B.; Barnes, W. L. *J. Phys. Chem. C* **2009**, *113*, 5120.
- (16) Link, S.; Wang, Z. L.; El-Sayed, M. A. *J. Phys. Chem. B* **1999**, *103*, 3529.
- (17) Haynes, C. L.; Van Duyne, R. P. *J. Phys. Chem. B* **2001**, *105*, 5599.
- (18) Jensen, T. R.; Malinsky, M. D.; Haynes, C. L.; Van Duyne, R. P. *J. Phys. Chem. B* **2000**, *104*, 10549.
- (19) Kelly, K. L.; Coronado, E.; Zhao, L. L.; Schatz, G. C. *J. Phys. Chem. B* **2003**, *107*, 668.
- (20) Jin, R.; Cao, Y. C.; Hao, E. C.; Métraux, G. S.; Schatz, G. C.; Mirkin, C. A. *Nature* **2003**, *425*, 487.
- (21) Xu, G.; Chen, Y.; Tazawa, M.; Jin, P. *J. Phys. Chem. B* **2006**, *110*, 2051.
- (22) Pinchuk, A.; Hilger, A.; von Plessen, G.; Kreibitz, U. *Nanotechnology* **2004**, *15*, 1890.
- (23) Haes, A. J.; Chang, L.; Klein, W. L.; Van Duyne, R. P. *J. Am. Chem. Soc.* **2005**, *127*, 2264.
- (24) Haes, A. J.; Van Duyne, R. P. *J. Am. Chem. Soc.* **2002**, *124*, 10596.
- (25) McMahon, J. M.; Wang, Y.; Sherry, L. J.; Van Duyne, R. P.; Marks, L. D.; Gray, S. K.; Schatz, G. C. *J. Phys. Chem. C* **2009**, *113*, 2731.
- (26) Malinsky, M. D.; Kelly, K. L.; Schatz, G. C.; Van Duyne, R. P. *J. Phys. Chem. B* **2001**, *105*, 2343.
- (27) Wang, Y.; Eswaramoorthy, S. K.; Sherry, L. J.; Dieringer, J. A.; Cadmen, J. P.; Schatz, G. C.; Van Duyne, R. P.; Marks, L. D. *Ultramicroscopy* **2009**, *109*, 1110.
- (28) Sohn, K.; Kim, F.; Pradel, K. C.; Wu, J.; Peng, Y.; Zhou, F.; Huang, J. *ACS Nano* **2009**, *3*, 2191.
- (29) Skrabalak, S. E.; Au, L.; Li, X.; Xia, Y. *Nat. Protoc.* **2007**, *2*, 2182.
- (30) Shukla, R. P.; Chowdhury, A.; Gupta, P. D. *Opt. Eng.* **1994**, *33*, 1881.
- (31) Sze, S. M. *Physics of Semiconductor Devices*; Wiley: New York, 1981.
- (32) Yoon, D. H.; Yoon, S. G.; Kim, Y. T. *Thin Solid Films* **2007**, *515*, 5004.
- (33) Taflove, A.; Hagness, S. C. *Computational Electrodynamics: The Finite-Difference Time-Domain Method*, 3rd ed.; Artech House, Inc.: Norwood, MA, 2005.
- (34) Gray, S. K.; Kupka, T. *Phys. Rev. B* **2003**, *68*, 045415.
- (35) Pecharroman, C.; Pérez-Juste, J.; Mata-Osoro, G.; Liz-Marzán, L. M.; Mulvaney, P. *Phys. Rev. B* **2008**, *77*, 035418.
- (36) Johnson, P. B.; Christy, R. W. *Phys. Rev. B* **1972**, *6*, 4370.
- (37) Mie, G. *Ann. Phys.* **1908**, *25*, 377.
- (38) Svedendahl, M.; Chen, S.; Dmitriev, A.; Käll, M. *Nano Lett.* **2009**, *9*, 4428.

JP104366R